CHIN. PHYS. LETT. Vol. 37, No. 8 (2020) 084202

# Multi-Core Conformal Lenses

Xinghong Zhu(朱星宏)†, Pengfei Zhao(赵鹏飞)†, and Huanyang Chen(陈焕阳)*

*Institute of Electromagnetics and Acoustics and Key Laboratory of Electromagnetic Wave Science and Detection Technology, Xiamen University, Xiamen 361005, China*

(Received 1 April 2020; accepted 4 June 2020; published online 28 July 2020)

We propose multi-core conformal lenses by combining conformal transformation optics with absolute instruments. Depending on the cores and incident angles, the conformal lenses have tunable functionalities like focusing, reflection, and transparency, thereby providing a feasible general method for designing multi-functional devices.

PACS: 42.15.Eq, 42.25.Bs, 42.15.Dp, 41.85.Lc DOI: 10.1088/0256-307X/37/8/084202

Gradient index (GRIN) lenses[1] have attracted a great deal of attention owing to their advantages in controlling light rays. Particularly, the Luneburg lens,[2] Eaton lens,[3] and invisible lens[4,5] are typical instruments of GRIN lenses with unique properties. They are referred to as absolute instruments (AIs)[6,7] for imaging that is free of geometrical aberration. The Luneburg lens can focus light rays from all directions on focal points, which lie in the direction of incidence and on the rim of the lens. Such a lens is broadly applied from microwave frequencies[8–12] to optical frequencies.[13] The Eaton lens reflects light rays to the incident direction-serving as a mirror. Its profile can be transmuted from that of the Luneburg lens by conformal mappings[14] and expended for imaging devices.[13,15] The invisible lens functions as a transparent device-guides light rays loop around its center to leave in the same direction where they incident; it plays a paramount role in omnidirectional invisibility cloaks. Its functionality can be realized by a combination of plane mirrors.[16] Recently, such lenses have been made equivalent to geodesic lenses in three-dimensional spaces for light trajectories.[17]

Transformation optics (TO)[18,19] are useful to control waves in designing functional devices such as invisibility cloaks,[20–22] rotators,[23] concentrators,[24,25] and illusion lenses.[26–30] In electromagnetic (EM) waves, most devices are anisotropic and inhomogeneous in electric permittivity or magnetic permeability tensors. Therefore, implementation is considerably challenging. Conformal transformation optics (CTO) was demonstrated to be more feasible in designing functional devices or lenses with simple refractive index profiles (RIPs) in required materials.[31,32] With TO, interesting implementations are carried out by AIs like a flattened Luneburg lens[10] and transmuted Eaton lens.[33] Based on the advantage of CTO, some interesting imaging devices were further designed[34,35] and introduced into invisibility cloaks[18] derived from AIs recently. Nowadays, optical waveguides play indispensable roles in communication systems. Some important multifunctionalities have been realized as integrated devices based on waveguides. For instance, photon sorting relies on different modes such as wavelength and polarization of light,[36] and nanoscale positions with a certain interval.[37] Moreover, two significant universal devices were fabricated successively based on waveguides. They are plasmonic NOR gates by the design of waveguide networks[38] and multimode waveguide crossing based on CTO.[39] Another novel device based on CTO was also realized in waveguides to illustrate self-focusing and the Talbot effect.[40] Devices from the fusion of CTO and AIs have potential for versatile functionalities and promising fabrications based on waveguides.

In this work, we design a new kind of multi-core conformal lenses based on AIs, which gives flexibility to manipulate the focusing, reflection, and transparency of light. Conventional AIs have single functions like omnidirectional focusing for the Luneburg lens, reflection for the Eaton lens, and transparency for the invisible lens, as mentioned above. The newly designed conformal lenses have multiple cores according to mappings. Different cores transformed by different AIs in one designed lens have different responses to fixed incident light rays, which stems from properties of the original AIs. Moreover, each core has diverse manipulations toward different angles of incident light, which is derived from the particular conformal mapping. In other words, the multi-core conformal lenses will show core-dependent manipulation if the light rays hit the lenses at a fixed angle. Meanwhile, they will also show direction-dependent manipulation if the light rays hit the lenses in different directions. Thus, these lenses have potential applications to detect the directions and split the light rays in different directions. We exemplify dual-core lenses

Supported by the National Natural Science Foundation of China (Grant No. 11874311).
†Xinghong Zhu and Pengfei Zhao contributed equally to this work.
*Corresponding author. Email: kenyon@xmu.edu.cn
© 2020 Chinese Physical Society and IOP Publishing Ltd

and triple-core lens to illustrate the functionalities of multi-core conformal lenses based on the Luneburg, Eaton, and invisible lenses. Furthermore, we give the rule of light trajectory changes in general multi-core conformal lenses for further design and applications.

We begin from the conformal power mapping:

$$w^N = z^N - 1, \tag{1}$$

where $N$ is an integer. Firstly, we introduce the mapping into CTO to produce the source illusion effect,[30] which can make one source appear as many in-phase sources and vice versa. It helps us produce $N$ cores in the lenses. We assume that there is a unit circle lens filled with AI profiles and surrounded by the air in $w$ space (see Fig. 1(a)). The refractive indices (RIs) are continuous in $w$ space. Using the mapping, we can get transformed shapes in $z$ space for $N = 2$ and 3, as in Figs. 1(b) and 1(c), respectively. Then, we can obtain the RIPs in $z$ space as $n_z = |dw/dz|\, n_w$ when we recall the basic principle of CTO.[18,32]

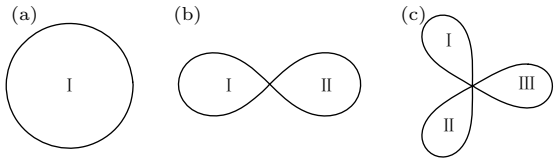


**Fig. 1.** (a) Unit circle lens in $w$ space. (b) Dual-core shape in $z$ space. (c) Triple-core shape in $z$ space.

Optical conformal mapping usually needs infinite-size materials to fill in the whole space. Notably, $w \to z$, when $z \to \infty$ for this mapping. We use a cut-off radius $r_c$ to convert the RIP in the region outside the transformed lens as the air,

$$n_z = \begin{cases} 1, & |z| > r_c, \\ |z^{N-1}|/|z^N - 1|^{1-\frac{1}{N}}, & |\sqrt{z^2-1}| > 1,\ |z| \leqslant r_c, \\ n_w \cdot |z^{N-1}|/|z^N - 1|^{1-\frac{1}{N}}|, & \sqrt{z^2-1}| \leqslant 1. \end{cases} \tag{2}$$

Sources illusion conformal lenses are set as $r_c = 5$. Also, they keep nearly the same functionalities as the full devices[30] for wave optics. Although RIs are discontinuous with the background in $r_c = 5$, this discontinuity barely influences the wave paths because RIs near $r_c = 5$ are approximately 1. In addition, trajectories of light rays are hardly influenced by this discontinuity throughout our simulations. By using the same conformal power mapping (Eq. (1)), we set multi-core conformal lenses as $r_c = 5$ for discussion. We will demonstrate wonderful functionalities of multi-core conformal lenses by our finite-size device. We produced all the emulational results by COMSOL Multiphysics (a commercial numerical software) to illustrate the functionalities by several examples for $N = 2, 3$. We utilize the geometrical optics interface, the radio frequency, EM waves, and frequency domain interface of the software to analyze the light ray trajectories and the RIs' distributions. In all simulations, we set the arbitrary unit of length as the meter.

We first consider $N = 2$ and suppose that lenses in $w$ space are Luneburg, Eaton, and invisible lenses with the profiles of $n_w(u, v) = \sqrt{2 - r_w^2}$, $n_w = \sqrt{2/r_w - 1}$ and $n(r_w) = [Q - 1/(3Q)]^2, Q = \sqrt[3]{-1/r_w + \sqrt{1/r_w^2 + 1/27}}$, where $r_w$ is the radial coordinate in $w$ space. Their corresponding transformed RIs in cores in $z$ space are

$$n_z(x, y) = \sqrt{\frac{2(x^2+y^2)}{\sqrt{(x^2-y^2-1)^2+4x^2y^2}} - (x^2+y^2)}, \tag{3}$$

$$n_z = \left\{ \frac{(x^2+y^2)}{\sqrt{(x^2-y^2-1)^2+4x^2y^2}} \cdot \left( \frac{2}{\sqrt[4]{(x^2-y^2-1)^2+4x^2y^2}} - 1 \right) \right\}^{1/2}, \tag{4}$$

$$n_z = \sqrt{\frac{x^2+y^2}{\sqrt{(x^2-y^2-1)^2+4x^2y^2}}} \left( Q - \frac{1}{3Q} \right)^2,$$

$$Q = \left\{ -\frac{1}{\sqrt[4]{(x^2-y^2-1)^2+4x^2y^2}} + \sqrt{\frac{1}{\sqrt{(x^2-y^2-1)^2+4x^2y^2}} + \frac{1}{27}} \right\}^{1/3}, \tag{5}$$

which are plotted in Fig. 2. The material inside the truncated boundary but outside the cores shares the same RI of

$$n = \sqrt{(x^2+y^2)/\sqrt{(x^2-y^2-1)^2+4x^2y^2}}.$$

We only need to change the RIs of the cores to change the functionalities of the whole lens. Thus, we labeled them as the dual-core Luneburg lens (DcL), the dual-core Eaton lens (DcE), and the dual-core invisible lens (DcI). The left and right cores of the lenses have the mirror-symmetric (or center rotation symmetric) RI distributions (seen from Eqs. (3)–(5)). In all ray-tracing simulations, we emit parallel light rays in the air outside the lenses. Figures 2(a)–2(c) individually show the detailed ray trajectories near the cores, and Figs. 2(d)–2(f) show the corresponding whole schematics of the dual-core lenses.

From Figs. 2(a) and 2(d), we observe that the left and right cores of the DcL will have different responses if light rays are incident at 45° (in green) or 135° (in blue). We analyze the case of 45° incidence to demonstrate this functionality. The rays going to the left core will directly focus on the mapped curve, while the rays going to the right core will turn around the singular point (−1,0) for 180° and then focus on the other side of the mapped curve. In addition, on the left core of the DcL, responses are dissimilar for the incidence of 45° and 135°. The rays coming from 135° will turn around the singular point (−1,0) for

180° and then focus on the front side of the mapped curve. In other words, one core has different manipulations toward different angles of incident light, which is different from the focusing property of the original Luneburg lens. This design may extend the application of the Luneburg lens in silicon photonics[13] and direction recognition detectors.

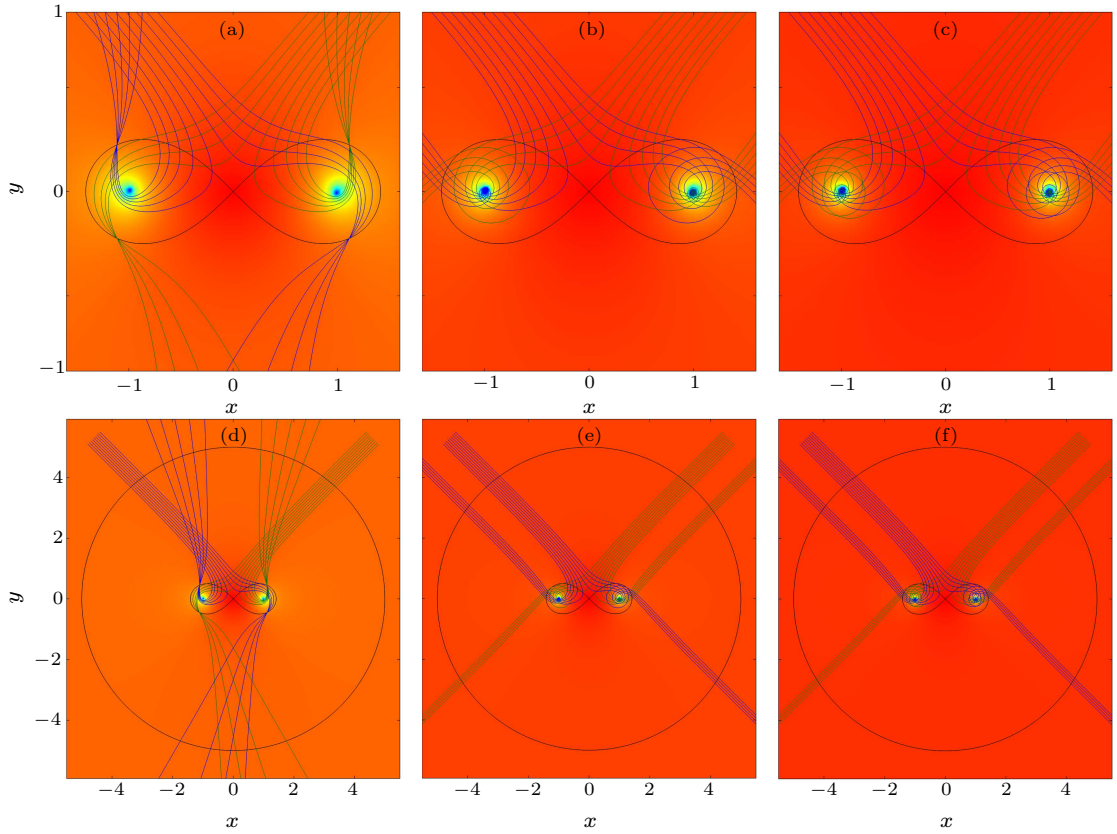


**Fig. 2.** RIPs of dual-core lenses and the trajectory of light rays manipulated by different cores. Light rays are released as parallel light at 45° (in green) and 135° (in blue). Ray trajectory near the cores for the (a) DcL, (b) DcE, and (c) DcI. Ray trajectory of the whole schematic with RI for (d) DcL, (e) DcE, and (f) DcI. In simulations, we set the arbitrary unit of length as the meter.

Similarly, we emit the light rays at angles of 45° (in green) and 135° (in blue) in air for the DcE. Its functionalities differ completely from those of the DcL. Observing the light trajectory of incidence from 45° in Fig. 2(e), the left core displays transparent and shifts light rays slightly, while the right core displays a reflector and guides the light rays back to the incident direction. If we magnify the view in Fig. 2(b), we can easily see that the light rays experience different paths with regard to the left and right cores. Light rays go through the left core with a loop rotation (360°), anticlockwise, and then propagate in the same direction as they hit the core. Ray trajectories revolve around the singular point (−1,0). Contrariwise, light rays go through the right core with one and a half loop rotations (540°), anticlockwise, and then back to the incoming direction. Meanwhile, this revolution of light rays is around the singular point (1,0). We recognize this as core-dependent manipulation. Now, we compare the differences in both the cores when the light rays come from different directions. Because the left and right cores show reverse functionalities to each other, we solely analyze the left core for further illustration. When the light rays coming from 45° hit the left core, they go through the core with an anticlockwise rotation, as described above. However, the light rays coming from 135° go through the left core with one and a half loop rotations (540°), clockwise, and then back to the incoming direction. We recognize this as direction-dependent manipulation.

So far, we have demonstrated that different cores of the DcE have different functionalities toward a fixed incidence of 45°. The left and right cores show the transparency and reflection, respectively. We have also demonstrated that each core of the DcE shows different manipulations depending on the incident angles. The left core shows the transparency for the incidence of 45°, while showing reflection for incidence of 135° instead. In summary, the DcE has controllable reflection and transparency that rely on two separate modes-core-dependent manipulation and direction-dependent manipulation. This design en-

riches the knowledge for designing a beam splitter based on the Eaton lens.

As the third example of a dual-core lens, we introduce the DcI and its functionalities. As shown in Fig. 2(f), for the light trajectory of incidence from 45°, the left core behaves similarly to that of the DcE, showing as transparent and shifting rays slightly. The right core also displays similarly, showing as a reflector and guiding the light rays back to the incident direction. However, light rays in the DcI follow diverse trajectories, which is different from the DcE. This is seen in the magnified view of Fig. 2(c). For the left core, light rays coming from 45° turn around the singularity point (−1,0) for 720°, anticlockwise, while for the right core, they turn around the singularity point (1,0) for 900°, anticlockwise. Moreover, each DcI core has different functionalities just like in the DcL and DcE. For incidence coming from 45°, light rays in the left core will be turned 720°, anticlockwise, and guided out in the same direction. However, for incidence coming from 135°, light rays in the left core will be turned 900°, clockwise, and guided back to the incoming direction. In summary, for fixed-angle incidence, reflection and transparency are shown as core-dependent manipulation. Meanwhile, for each core, reflection and transparency are shown as direction-dependent manipulation. This new design adds reflection for the DcI lens, compared with the traditional invisible lens, and changes it into transparency by changing the incident angles of light rays. The conformal lens can also be used as a beam splitter, depending on the angle of incidence.

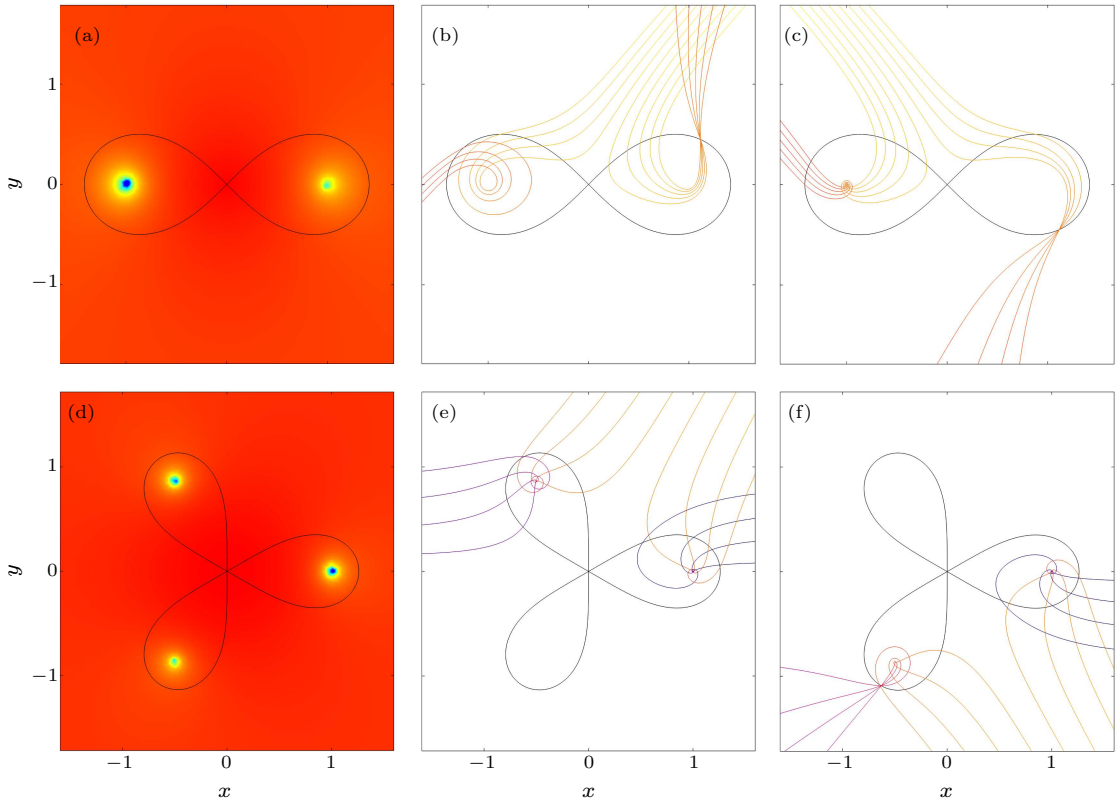


**Fig. 3.** RI of (a) combined dual-core Eaton–Luneburg lens and (d) combined triple-core Eaton–Luneburg–invisible lens. Ray-tracing simulations for light rays incident at angles of (b) 45°, (c) 135°, (e) 60° and (f) −60° for them. In simulations, we set the arbitrary unit of length as the meter.

Since the multi-core conformal lenses have core-dependent manipulations, we further discuss the combined functionalities depending on the combination of different cores. We introduce a dual-core Eaton–Luneburg lens (DcEL) for $N = 2$ and a triple-core Eaton–Luneburg–invisible lens (TcELI) for $N = 3$ on this issue. In addition, we separately depict the RIPs and light trajectories to observe details inside the cores. The DcEL, where the left and right cores are transformed Eaton and Luneburg lenses, respectively, has the RI shown in Fig. 3(a). For light rays coming from 45°, the left core rotates the light rays for 360° and guides them to the direction of 225°, while the right core focuses on the light rays at the mapped curve with 180° rotation. For the incidence of 135°, the left core reflects the light rays with a 540° rotation inside the core, while the right core focuses on the light rays at the mapped curve. Thus, by combination, we realized focusing, reflection, and transparency in one lens.

Now we consider a more general case, the TcELI. Cores I, II, and III are transformed Eaton, Luneb-

urg, and invisible lenses, respectively. Figure 3(d) shows its distributions of RI. If the incidence comes from 60°, light rays in core I travel around the point $(-1/2, \sqrt{3}/2)$ for 660°, anticlockwise, and then propagate into the 180° direction; while light rays in core Ⅲ rotate around the singular point (1,0) for 1320°, clockwise, and then propagate to the 0° direction. If the incidence comes from −60°, light rays in core Ⅲ will loop around the point (1,0) for 1320°, anticlockwise, and then propagate into the 0° direction; while light rays in core Ⅱ will turn around the point $(-1/2, -\sqrt{3}/2)$ for 240°, clockwise, and then focus at the mapped curve. The flexibility of the angle choices when we set $N = 3$ gives the focusing, reflection, and transparency.

In fact, we can obtain a conformal lens with $N$ cores and $N$ singular points ($z = e^{i2\pi j/N}$ ($j = 0, 1, \ldots, N-1$)). More combinations of the cores can be obtained within one lens to produce more functionalities. The deflection angle $\theta_z$ at which light rays travel through the multi-core conformal lenses is not random. It is related to the number of times $T$ during which light rays pass the branch cuts[18,30,32] in $w$ space (virtual space) and follows:

$$\theta_z = \theta_w + 360^\circ T(N-1)/N, \tag{6}$$

where $N$ is the exponent of the conformal power mapping, and $\theta_w$ characterizes the deflection angle that light rays through $w$ space. For $N = 2$, the branch cut is the line from $w = -i$ to $w = i$, $\theta_z = \theta_w + 180^\circ T$. For the DcE, $\theta_w = 180°$, and $T = 1$ or 2, so the lens will guide light rays to loop the singular point for 360° or 540°. For the DcI, $\theta_w = 360°$, $T = 2$ or 3. Accordingly, $\theta_z = 720°$ or 900°. In the case of $N = 3$, the branch cuts in $w$ space are lines from the origin to $z = e^{i(2j+1)\pi/3}$ ($j = 0, 1, 2$), and $\theta_z = \theta_w + 240^\circ T$.

In conclusion, we have designed a new class of multi-core conformal lenses, which have tunable functionalities using conformal power mapping based on AIs. Different cores have different functionalities such as focusing, reflection, and transparency toward a fixed-angle incidence. Meanwhile, each core has different manipulations depending on the incident angles. The combination of different functional cores in one lens can produce more functionalities as well. The recent great progress in designing a self-focusing conformal lens,[40] which was constructed by GRIN micro-structured optical waveguide, paving the way for realizing multi-core conformal lenses. It is not difficult to foresee broad implementations for conformal lenses as direction recognition detectors and beam splitters. Riemann's analysis[18,30,32] is used to evaluate the angle that light rays travel through the lenses. In addition, our method of designing multi-core lenses could be general. For instance, we may design a multi-core Maxwell's fish-eye lens based on conformal power mapping. Furthermore, $N$ can be a non-integer or even an irrational number (e.g., $\pi$), which may have more interesting functionalities.

## References


[1] Gomez-Reino C, Perez M V and Bao C 2002 *Gradient-Index Optics: Fundamentals and Applications* (Berlin: Springer)
[2] Luneburg R K 1964 *Mathematical Theory of Optics* (California: University of California Press)
[3] Eaton J E 1952 *Transactions of the IRE Professional Group on Antennas and Propagation* **4** 66
[4] Hendi A, Henn J and Leonhardt U 2006 *Phys. Rev. Lett.* **97** 073902
[5] Minano J C 2006 *Opt. Express* **14** 9627
[6] Born M and Wolf E 2006 *Principles of Optics* (Cambridge: Cambridge University Press)
[7] Tyc T, Herzanova L, Sarbort M *et al.* 2011 *New J. Phys.* **13** 115004
[8] Cornbleet S 1976 *Microwave Optics: The Optics of Microwave Antenna Design* (San Diego: Academic Press)
[9] Skolnik M I 2000 *Introduction to Radar Systems* (New York: McGraw-Hill)
[10] Kundtz N and Smith D R 2010 *Nat. Mater.* **9** 129
[11] Ma H F and Cui T J 2010 *Nat. Commun.* **1** 124
[12] Dockrey J A, Lockyear M J and Berry S J *et al.* 2013 *Phys. Rev. B* **87** 125137
[13] Zentgraf T, Liu Y M, Mikkelsen M H *et al.* 2011 *Nat. Nanotechnol.* **6** 151
[14] Leonhardt U and Thomas P 2010 *Geometry and Light: The Science of Invisibility* (New York: Dover Publications Inc.)
[15] Smolyaninova V N, Smolyaninov I I, Kildishev A V *et al.* 2010 *Opt. Lett.* **35** 3396
[16] Perczel J, Tyc T and Leonhardt U 2011 *New J. Phys.* **13** 083007
[17] Xu L, Wang X, Tyc T *et al.* 2019 *Photon. Res.* **7** 1266
[18] Leonhardt U 2006 *Science* **312** 1777
[19] Pendry J B, Schurig D and Smith D R 2006 *Science* **312** 1780
[20] Schurig D, Mock J J, Justice B J *et al.* 2006 *Science* **314** 977
[21] Schurig D, Pendry J B and Smith D R 2006 *Opt. Express* **14** 9794
[22] Chen H Y, Yang T, Luo X D *et al.* 2008 *Chin. Phys. Lett.* **25** 3696
[23] Chen H Y and Chan C T 2007 *Appl. Phys. Lett.* **90** 241105
[24] Rahm M, Schurig D, Roberts D A *et al.* 2008 *Photon. Nanostruct. Fundam. Appl.* **6** 87
[25] Sadeghi M M, Nadgaran H and Chen H Y 2014 *Front. Phys.* **9** 90
[26] Lai Y, Ng J, Chen H Y *et al.* 2009 *Phys. Rev. Lett.* **102** 253902
[27] Jiang W X and Cui T J 2010 *Opt. Express* **18** 5161
[28] Jiang W X, Ma H F, Cheng Q A *et al.* 2010 *Opt. Express* **18** 11276
[29] Xu Y D, Du S W, Gao L *et al.* 2011 *New J. Phys.* **13** 023010
[30] Chen H Y, Xu Y D, Li H *et al.* 2013 *New J. Phys.* **15** 093034
[31] Li J S and Pendry J B 2008 *Phys. Rev. Lett.* **101** 203901
[32] Xu L and Chen H Y 2015 *Nat. Photon.* **9** 15
[33] Ma Y G, Ong C K, Tyc T *et al.* 2009 *Nat. Mater.* **8** 639
[34] Chen H Y 2018 *Phys. Rev. A* **98** 043843
[35] Tao S C, Zhou Y Y and Chen H Y 2019 *Phys. Rev. A* **99** 013837
[36] Laux E, Genet C, Skauli T *et al.* 2008 *Nat. Photon.* **2** 161
[37] Hu Q, Xu D H, Zhou Y *et al.* 2013 *Sci. Rep.* **3** 3095
[38] Wei H, Wang Z, Tian X *et al.* 2011 *Nat. Commun.* **2** 387
[39] Li S, Zhou Y Y, Dong J J *et al.* 2018 *Optica* **5** 1549
[40] Wang X, Chen H Y, Liu H *et al.* 2017 *Phys. Rev. Lett.* **119** 033902